Interfacial plasmon at a singular solid-liquid interface in a partially molten aluminum alloy

Prakash Palanisamy,[1] Wilfried Sigle,[2,*] and James M. Howe[1,†]

[1]*Department of Materials Science and Engineering, University of Virginia, 395 McCormick Road, Charlottesville, Virginia 22904, USA*

[2]*Max Planck Institute for Intelligent Systems, Heisenbergstrasse 3, 70569 Stuttgart, Germany*

(Received 9 January 2012; published 4 May 2012)

Nanoplasmonics is an important emerging research area in technologies, such as energy conversion using photovoltaic devices and hydrogen sensing using Pd nanoparticles. So far, plasmon excitations are only known to exist at the interface between two different dielectric media, such as two solids or at solid-vacuum surfaces. There has been no evidence for the presence of a plasmon at a solid-liquid interface. This paper presents results on the existence and nature of the plasmon resonance between a semiconducting solid and a liquid metal, investigated in a transmission electron microscope having sub-eV and sub-Å resolutions. The results are compared with calculations of the plasmon based on dielectric theory and are corroborated with energy-filtered imaging analyses. The unique plasmon resonance observed at the solid-liquid interface provides new insight into the behavior of plasmons in research areas from biomedical imaging to liquid crystals, including the technologies mentioned above.

DOI: 10.1103/PhysRevB.85.195305 PACS number(s): 73.20.Mf, 81.05.Bx, 73.20.Jc

I. INTRODUCTION

Plasmon excitations are important phenomena both scientifically and technologically. For example, the discovery of surface plasmons and the realization that they can be manipulated in small structures has led to the current important field of nanoplasmonics.[1–5] Similarly, it has been recognized for some time that plasmons can exist at internal surfaces or interfaces, such as between two solids,[6,7] and there is experimental evidence for this in metal alloys and semiconductor systems.[8–10] Whether plasmons exist and can be detected at a solid-liquid interface remains an unanswered question. There is a potential application for this in cancer therapy where the body fluid/Au layer interaction[11] is critical, for example.

Dielectric theory places no restrictions on the state of two materials present across an interface and, therefore, predicts that a unique plasmon should be present at a solid-liquid interface. Furthermore, one expects the valence/conduction electrons at the solid-liquid interface to be different than in either of the bulk phases due to differences in the Fermi energies of the materials, potential ordering in the first several layers of the liquid, as well as any composition gradients that may exist at the interface.[12–16] Hence, the collective oscillations of these electrons should be different, although they may be delocalized. Unfortunately, given these expectations, it is very difficult to investigate the solid-liquid interface experimentally, particularly in inorganic materials because the materials are opaque, must be heated to melting, require an experimental technique that has high spatial resolution, etc. Despite these difficulties, progress has been made in observing solid-liquid interfaces in organic and inorganic materials using high-resolution transmission electron microscopy (TEM),[13,14,16,17] scanning probe microscopy,[18] and synchrotron x-ray scattering.[12,19,20]

With the availability of electron-beam instruments with sub-eV and sub-Å resolutions, one can explore the physical,[21,22] mechanical,[21] and optical[1,2] properties of materials with unprecedented spatial resolution. A striking example of this is the recent work by Nelayah *et al.*[2] using electron energy-loss spectroscopy (EELS) in a TEM to investigate the surface plasmons on Ag nanoparticles. In contrast, the fundamental plasmon physics in liquid metals, and more specifically, the behavior of free electrons at the interface between a liquid metal and a semiconducting solid is largely unknown. The interface between a metal and a semiconductor (the so-called Schottky junction[23]) is technologically important in microelectronics since it controls the electrical transport properties in semiconductor devices. While sophisticated experiments[24] and theories[25] have explored the electrical,[26] thermal,[27] and optical[28] properties of such interfaces, only a few papers have explored the interface between a liquid metal and a semiconducting material, such as Si.[12] The current paper investigates the interfacial plasmon present between molten Al-Si alloys in contact with a singular Si interface using *in situ* valence EELS in the TEM.[29]

II. EXPERIMENTAL PROCEDURE

Atomized Al-17.8Si-1.8Cu-0.6 Mg alloy in powder form was supplied by Valimet, Inc. Some 0.5 g of the powder sample was added to 25 ml of ethanol and was ultrasonicated for 1 h to disperse the aggregated particles. The solution was left undisturbed for 24 h to allow the larger-sized particles to settle. The remaining particles were collected near the top of the suspension using a pipette and were deposited on an ultrathin holey carbon support film on a 200-mesh Cu grid obtained from Ted Pella, Inc.

A JEOL-JEM 2010F TEM with a Schottky field-emission gun operating at 200 kV and having a postcolumn Gatan imaging filter (GIF-Model 652) was used to acquire the low energy-loss spectra from a pure liquid Al particle at 700 °C. The energy resolution measured from the full width at half maximum (FWHM) of the zero-loss peak was 1.1 eV. DIGITAL MICROGRAPH software was used to acquire and to process the energy-loss spectra to obtain the energy dependence of real (ε_1) and imaginary (ε_2) parts of the dielectric constant through Kramers-Kronig analysis[30] after plural scattering removal by Fourier-logarithm deconvolution.[30]

A Gatan double-tilt heating holder was used to resistively heat the sample to 590 °C where the solid Si is in contact

with the liquid Al alloy at this temperature, and a Pt/Pt-13%Rh thermocouple in contact with the furnace provided the specimen temperature to within ±15 K. A bright-field TEM image and diffraction patterns from the Si and liquid Al phases were acquired to determine that the Si facet in contact with the liquid Al was {111}.

The Zeiss sub-eV sub-Å microscope (SESAM) with a Schottky field-emission gun operating at 200 kV, fitted with a Collected Electron Optics Systems ω-type monochromator, Koehler illumination, and an in-column Mandoline energy filter was used to acquire the low-loss spectra across the solid-liquid interface and from a Si single crystal close to a ⟨100⟩ zone axis at 590 °C, and this was processed through DIGITAL MICROGRAPH software to obtain the real (ε_1) and imaginary (ε_2) parts of the dielectric constant. The energy resolution measured at the FWHM of the zero-loss peak was 0.14 eV. The collection half-angle was limited to 6 mrad using an objective aperture.

A low-loss spectrum image was acquired in the scanning TEM mode of the SESAM TEM using a probe size of 0.6 nm and stepping 35 nm across the singular solid Si-liquid Al interface in 0.8-nm increments. A total of 45 spectra was acquired using the autoacquisition mode with an acquisition time of 2 s for each spectrum. The inelastic mean-free-path lengths of Al and Si are 142 and 139 nm, respectively, at 200 kV. A particle size of ∼150 nm was chosen for the present paper, and this leads to multiple plasmon peaks from the Si and liquid Al phases. These are useful for accurately calibrating the plasmon energies. An energy dispersion of 0.018 eV/channel for spectrum image acquisition allowed the Si, liquid Al, and the interface plasmon energies to be measured with high accuracy. A series of energy-filtered TEM (EFTEM) images was acquired in a charge-coupled device 2048 × 2048-pixel camera using a 0.2-eV energy slit taken 0.2 eV apart from 12.5 to 17.7 eV across the plasmon energies of Si to liquid Al. Due to fourfold binning of the camera, the effective pixel size in the EFTEM image is 0.89 × 0.89 nm. A total of 26 EFTEM images was acquired with an acquisition time of 10 s. The spatial drift of the energy-filtered images was corrected using an auto-cross-correlation script developed by Schaffer *et al.*[31] The multivariate statistical analysis software plug-in in DIGITAL MICROGRAPH was used for processing the EFTEM images. This allows one to obtain an improved signal-to-noise ratio in the images and is based on a principal component analysis. The data were reconstructed using four statistically significant principal components.[32]

III. RESULTS AND DISCUSSIONS

Valence-electron energy-loss spectroscopy and EFTEM were performed on a partially molten Al-Si-Cu-Mg alloy particle in a Zeiss SESAM operated at 200 kV. A bright-field TEM image of the particle taken at 590 °C is shown in Fig. 1(a). The particle contains two phases, Si, which displays a prominent {111} facet, in contact with liquid Al containing ∼8 at. % Si in solution as expected from the equilibrium phase diagram.[33] The EELS spectrum image shown in Fig. 1(b) was acquired by stepping a 0.6-nm diameter electron probe from the liquid Al across the solid-liquid interface and into the Si [dotted line in Fig. 1(a)] in 0.8-nm increments for a total distance of 35 nm. Figures 1(c) and 1(d) show the energy dependence of the real (ε_1) and imaginary (ε_2) parts of the complex dielectric constants of liquid Al and solid Si, respectively. These data were used to calculate valence-electron energy-loss spectra (plasmons) across the solid-liquid interface using Eq. (1).

The relatively narrow high-intensity spectral feature in Fig. 1(b) is due to the volume plasmon excitation in liquid Al corresponding to an energy-loss of 14.2 eV, and the low-intensity broader spectral feature is the volume plasmon from Si at 16.3 eV. The volume plasmon energy of solid Al at room temperature is ∼15.3 eV,[30] and the lower plasmon energy measured in liquid Al is due to the increased atomic volume in the liquid phase, i.e., expansion on melting (in the jellium model,[30] the volume plasmon energy of a nearly free-electron metal, such as Al is proportional to the valence-electron density). This is consistent with previous papers on liquid Al.[34,35] A unique plasmon feature corresponding to the interface between the crystalline Si and liquid Al is clearly visible in the spectrum image in Fig. 1(b). To corroborate this result, complimentary theoretical calculations based on the dielectric theory and EFTEM imaging analyses were performed.

The energy-loss (scattering) probability of a fast moving electron with velocity v traveling parallel to a planar interface with normal x between two materials as a function of frequency ω is given by[36]

$$\frac{dP(x)}{d\hbar\,\omega} = \frac{e^2}{2\pi^2\varepsilon_0\hbar^2v^2}\left[\ln\frac{q_c v}{\omega}\,\mathrm{Im}\left\{-\frac{1}{\varepsilon_1(\omega)}\right\} + K_0\left(\frac{2\omega b}{v}\right)\times\left(\mathrm{Im}\left\{-\frac{2}{\varepsilon_1(\omega)+\varepsilon_2(\omega)}\right\} - \mathrm{Im}\left\{-\frac{1}{\varepsilon_1(\omega)}\right\}\right)\right], \tag{1}$$

Where, in the present investigation, $\varepsilon_1(\omega)$ and $\varepsilon_2(\omega)$ are the complex dielectric functions of liquid Al and Si. The imaginary terms $\mathrm{Im}(-\frac{1}{\varepsilon_1(\omega)})$ and $\mathrm{Im}(-\frac{2}{\varepsilon_1(\omega)+\varepsilon_2(\omega)})$ are the energy-loss functions that define the shape of the volume plasmons of Si and liquid Al and the interface plasmon, respectively. K_0 is a modified Bessel function that describes the contributions of the volume plasmons from liquid Al and Si for an electron beam at a distance b (impact parameter) from the interface, and q_c is the critical wave vector (1.19 nm^{-1}).

Figure 2(a) shows a schematic near the interface with arrows indicating the locations where experimental spectra (slices 12 to 24) and calculated spectra [using Eq. (1) with distance b in 1.6-nm increments] were compared across the liquid Al-Si{111} interface. The plasmon energy and the FWHM of the liquid Al plasmon in slices 12, 14, and 16 compare well with the calculated spectra as shown in Figs. 2(b)–2(d). The FWHM measured for the liquid Al plasmon is 1.85 eV, which is higher than the half-width of 0.5 eV for solid Al,[37] indicating that damping of the plasmon in liquid Al is faster[35] than in the solid. Interface slice 18 in Fig. 2(e) (and, to a lesser extent, slice 16) exhibits an asymmetric tail on the high-energy side. This asymmetry could be an inherent feature of the solid-liquid interface plasmon and/or attributed to electron-phonon interactions that occur during high-temperature EELS studies involving molten liquids.[35]

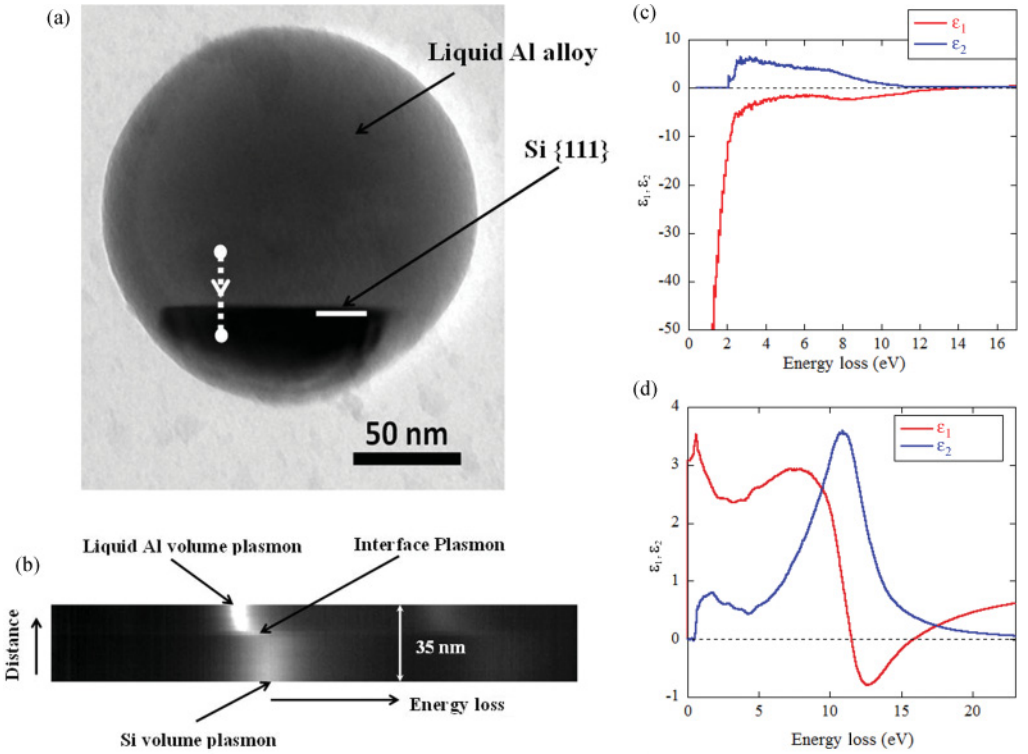

FIG. 1. (Color online) Bright-field TEM image and corresponding EELS spectrum image taken across the solid Si-liquid Al interface of an Al-Si alloy particle at 590 °C. (a) Bright-field TEM image of a partially molten Al-Si alloy particle taken at 590 °C showing a singular Si{111} interface in contact with a liquid Al alloy. (b) EELS spectrum image corresponding to a 35-nm distance across the solid-liquid interface. (c) Energy dependence of the real (ε_1) and imaginary (ε_2) parts of the dielectric constants of liquid Al and (d) solid Si.

Comparing the experimental spectra on the Si side (slices 20, 24, and 26) with the calculated ones in Figs. 2(f)–2(h) shows that the calculated spectra display a lower plasmon energy than the experimental spectra, i.e., close to that of the plasmon energy in interface slice 18. With increasing distance away from the interface, the plasmon peak progressively moves until it is coincident with the experimental spectrum in slice 26. Thus, an *e* beam located 4.8 nm away from the interface only excites the volume plasmon of Si. When the electron beam is closer to the interface than this, the excitation probability of the interface plasmon is higher on the Si side than on the liquid Al side (the well-known Begrenzungs effect[8,9,38]), and this reduces the volume plasmon of Si relative to the interface plasmon.

Since the electron beam has a finite size of 0.6 nm and it broadens as it travels through the particle, when the beam is on or near the interface, there is a probability of exciting volume plasmons from both liquid Al and solid Si. In addition, there is some delocalization of the plasmon excitation due to the inelastic-scattering process.[30,39] Therefore, the interface spectrum (slice 18) has relative contributions from both liquid Al and Si plasmons but can be deconvoluted based on the measured plasmon energies of liquid Al and crystalline Si, which are 14.4 and 16.3 eV, respectively. Since the electron-plasmon interaction in a material can be described as a quantum harmonic oscillator,[5,40] the plasmon peak can be appropriately fitted by a Lorentzian function. The experimental and calculated plasmon energies and the FWHM of liquid Al, crystalline Si, and the interface plasmon were extracted by fitting Lorentzian functions[32] to the plasmon peaks, and these are given in Table I. The experimental and calculated results agree within ±0.2 eV. Figure 2(i) shows the deconvolved contributions of the Si, Al, and interface plasmon peaks to the total interface spectrum 18. For comparison, the experimental spectrum and the summation of all the individual plasmon contributions are also shown. The summation of all the plasmon contributions matches the experimental spectrum well.

Figure 3(a) shows normalized low-loss spectra near the interface region. The spectra were displaced at regular intervals along the ordinate for comparison. Solid lines correspond to the peak centers of the liquid Al and crystalline Si volume plasmons at 14.4 and 16.3 eV, respectively, and the interface plasmon peak in the spectrum (arrow on left) is visible at an energy loss of 15.5 eV as indicated by a dotted line. The interface plasmon energy of solid Si/liquid Al is lower as compared to solid Si/solid Al and is attributed due to the change in the liquid Al plasmon energy as solid Si plasmon energy does not change with temperature.[10,32,35] To substantiate the presence of a unique plasmon peak between the solid Si and the liquid Al plasmons, EFTEM images were acquired using a 0.2-eV energy slit scanning from 12.5 to 17.7 eV in 0.2-eV increments to obtain 26 images. In order to obtain a high signal-to-noise ratio in the images, a multivariate statistical analysis based on principal component analysis was performed.[41,42] A tableau of selected EFTEM images is shown in Fig. 3(b) with the energy-loss values indicated on the image. The bright phase in the 14-eV image corresponds to liquid Al,

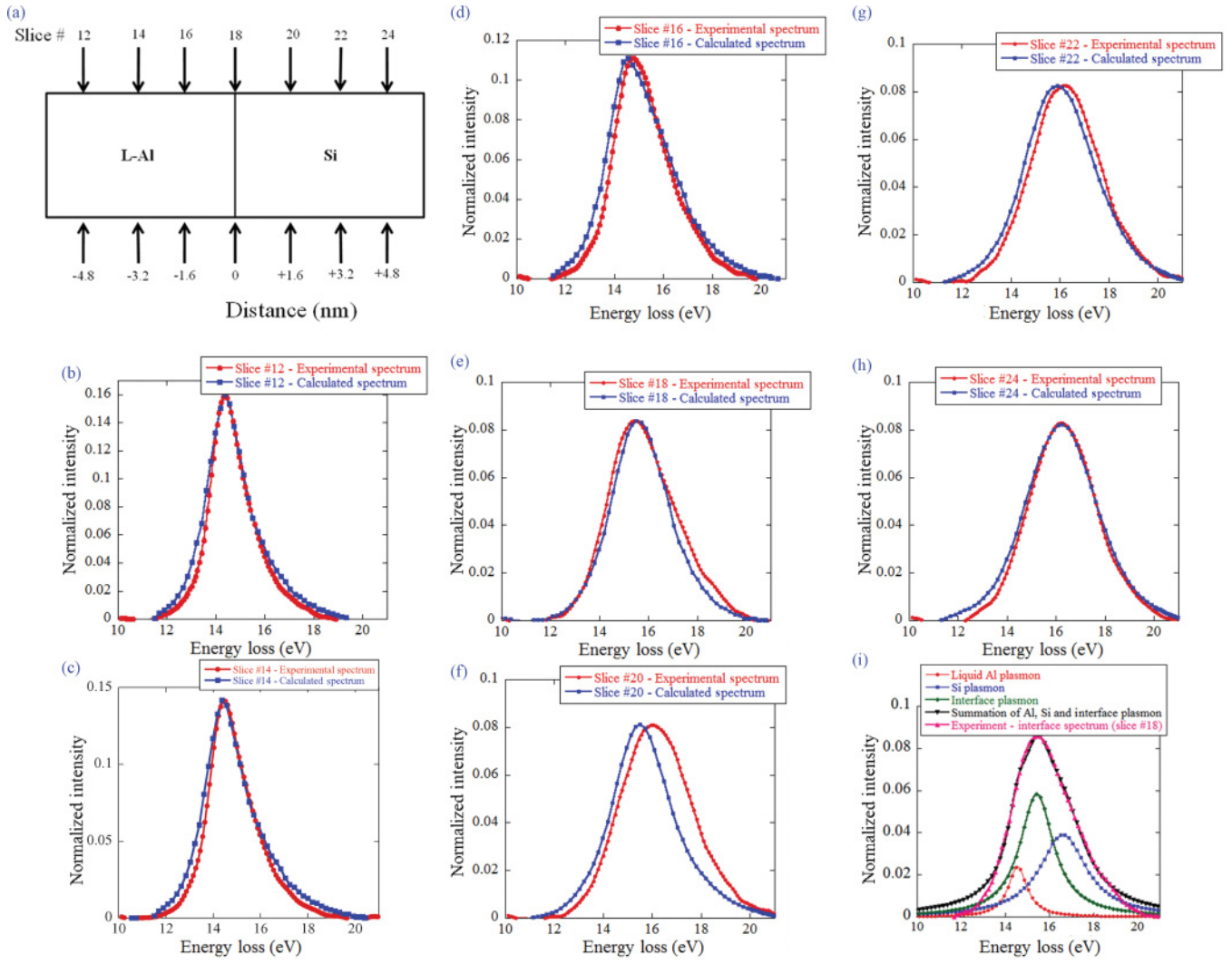

FIG. 2. (Color online) Comparison between experimental and calculated EELS spectra across the solid Si-liquid Al interface. (a) Schematic of a thin specimen showing the locations across the solid-liquid interface where experimental spectra (slices) were compared with calculated spectra. (b)–(h) Comparison between experimental and calculated EELS spectra at different impact parameters, i.e., distances from the interface. (i) Deconvolution of the interface spectrum showing the relative contributions of the volume plasmons of Si, liquid Al, and the interface plasmon.

and this brightness persists at higher-energy losses due to the broad nature of the liquid Al plasmon peak. The Si phase becomes bright at 16.5 eV, although its intensity is not even because the Si is oriented along a ⟨110⟩ zone axis, and strong Bragg diffraction is contributing to the contrast in the EFTEM image. In the 15.5- and 16-eV images, the interface is brighter than either of the liquid Al or Si phases, further validating the presence of a plasmon peak/signal between the volume plasmons of Si and liquid Al in the experimental spectrum. A naturally formed oxide layer ∼7 nm is also visible in the image, and this prevents the liquid Al from evaporating into the microscope column. These results demonstrate that the valence-electron density at the solid-liquid interface is different from either the bulk Al or Si, and that an interfacial plasmon resonance can be imaged when excited by an electron beam. Interfacial plasmons have been previously observed

TABLE I. The plasmon energies and FWHM of liquid Al, the interface, and Si, extracted by fitting a Lorentzian function to the experimental and calculated spectra.

	Plasmon energy (eV)		Full width at half maximum (eV)	
	Experiment	Calculation	Experiment	Calculation
Liquid Al	14.3	14.4	1.8	2.0
Interface	15.4	15.6	3.1	2.9
Si	16.2	16.2	3.3	3.4

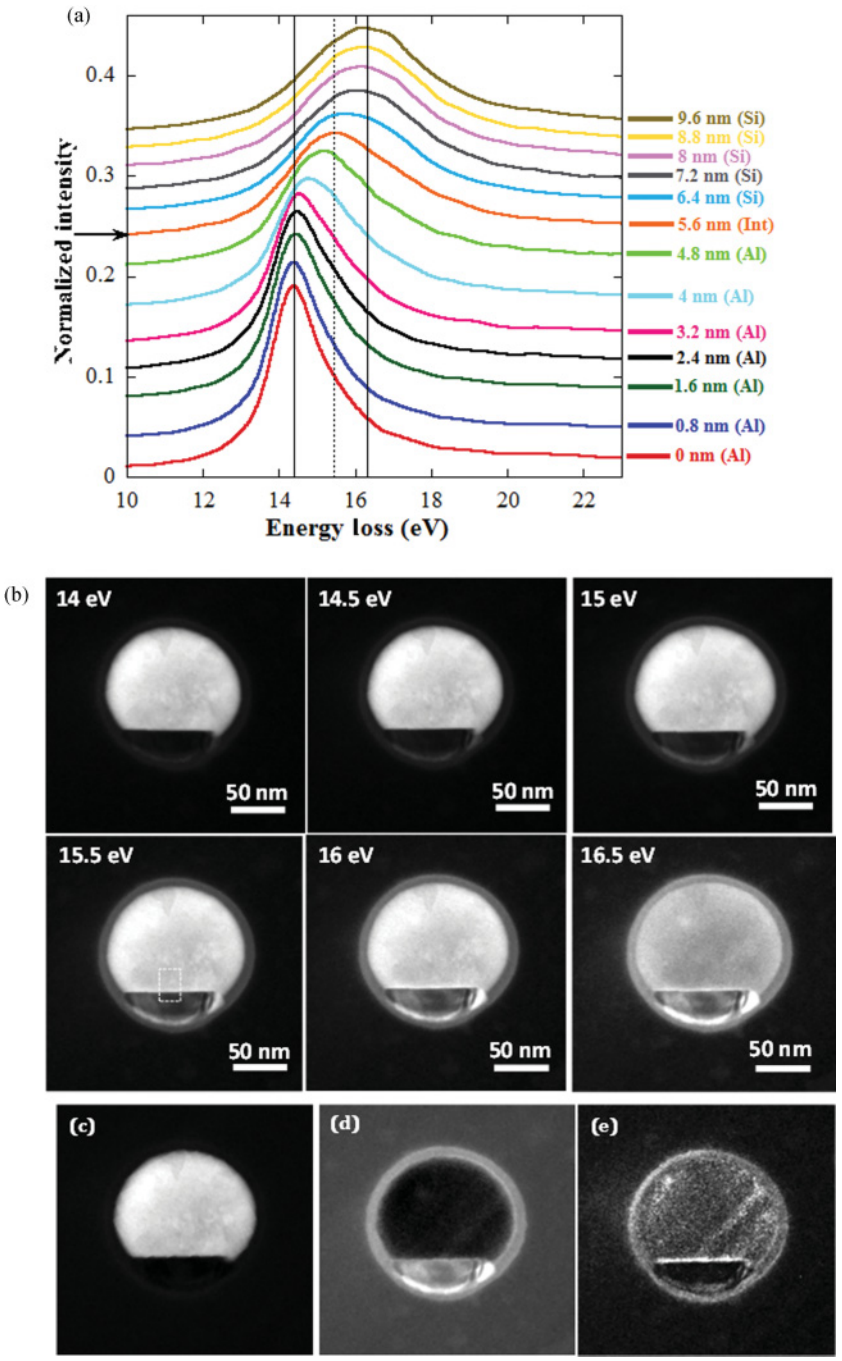

FIG. 3. (Color online) Normalized experimental EELS spectra across the solid-liquid interface and EFTEM analyses. (a) EELS spectra near the solid-liquid interface, the vertical solid lines correspond to the peak centers of the volume plasmons of liquid Al and Si at 14.4 and 16.3 eV, respectively. The dashed line corresponds to the peak center of the interface plasmon at 15.5 eV. The arrow on the left side indicates the interface. (b) Tableau of the EFTEM images acquired using a 0.2-eV energy slit with the energy-loss values indicated on the images. The images were reconstructed after multivariate statistical analysis to improve the signal-to-noise ratio. (c) MLLS fit coefficient map of liquid Al. (d) MLLS fit coefficient map of Si. (e) Reduced χ^2 map of the interface.

at solid-solid interfaces[8,9] and solid-vacuum[3,4,6] interfaces in thin films and small particles but not at a solid-liquid interface.

Multiple linear least-squares (MLLS) fitting[30] was performed on the reference spectra from liquid Al and Si in the energy range of 12.5 to 17.5 eV. Figures 3(c) and 3(d) show the MLLS fit coefficient maps, and the bright phases in the images correspond to the liquid Al and Si, respectively. Figure 3(e) shows the reduced χ^2 fit map obtained by the MLLS fitting, which reveals the interface plasmon component. This additional result also corroborates the plasmon peak observed at the interface between solid Si and liquid Al in the experimental spectrum image in Fig. 1(a) and in the EELS spectra in Fig. 3(a).

Figure 4 shows an average intensity profile taken across the solid-liquid interface from the 15.5-eV EFTEM image (the dotted rectangular box) in Fig. 3(b). The intensity on the liquid Al and Si sides (shown with horizontal dotted lines) is almost constant; therefore, the peak width in the intensity profile corresponds to the plasmon signal at the solid-liquid interface. The background intensity profile on the Si side was matched to that of the Al side by removing 1 nm and shifting it vertically to yield an approximately Gaussian function of the plasmon signal at the solid-liquid interface. The peak half-width measured from the profile was ~5.5 nm.

This value is substantially larger than the width of any ordered liquid layers of ~2 nm found at the Al-liquid Si[43]

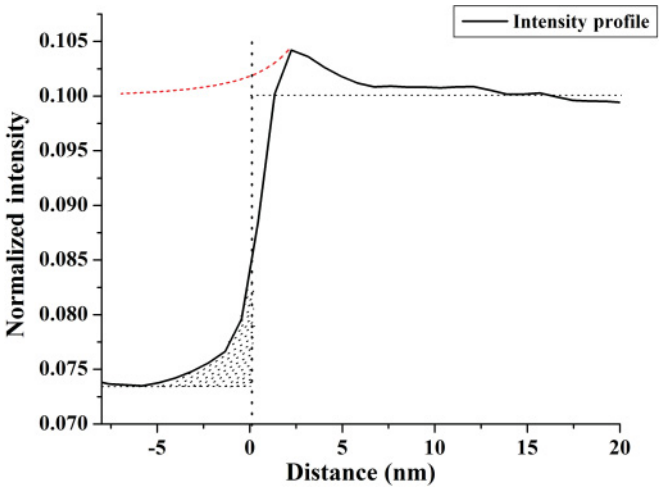

FIG. 4. (Color online) Intensity profile across the solid-liquid interface. The average intensity profile from the dotted rectangular box across the solid-liquid interface in the 15.5-eV EFTEM image in Fig. 3(b). The horizontal dotted lines represent the background on the liquid Al and Si sides. The dashed red curve is the background shifted from the Si side to match that of the Al side minus 1 nm of intensity to the left of the vertical dashed line (hatched region) that was removed so the background intensities are the same on the Al and Si sides.

and Si-liquid Pb[12] interfaces. This difference is likely due to the delocalization of the excitation process of the plasmon at the interface,[30,39,44] which is an inherent nature of the inelastic scattering of electrons at energy losses less than ~100 eV. It is worth mentioning that, in the present experiments, the spatial resolution in EFTEM mapping[45] is not limited by chromatic aberration because of the use of narrow energy slits and the observation of small energy losses (<100 eV). Also, nonisochromaticity is negligible (<10 meV across the Al-Si particle) because of the use of a high-transmissivity energy filter.[46] Therefore, the plasmon signal at the interface can be entirely accounted for by delocalization of the inelastic scattering of electrons. Although the ordering of atoms in the liquid at the solid-liquid interface[13–15] could change the free-electron density and, hence, the signal from the interface, this effect is likely overshadowed by the delocalization of scattering.

IV. CONCLUSION

The experimental results and theoretical calculations presented herein provide convincing evidence for the existence of a unique plasmon state at a singular solid-liquid interface. Although this interface plasmon can be predicted by dielectric theory, the present paper provides detailed information on its characteristics and behavior at the interface as well as direct evidence that the free-electron density at the interface is different from the bulk phases. EFTEM image analyses indicated that the electron excitations at the interface are delocalized to within about 5.5 nm. The present paper on the interfacial plasmon behavior between Si and liquid Al provides further insight into phenomena important to the active research area of nanoplasmonics, such as in biomedical imaging of body fluid and Au nanoparticle interactions for cancer therapy[11] and potentially in liquid crystals, for example.

ACKNOWLEDGMENTS

The authors (P.P. and J.M.H.) gratefully acknowledge support of this research by the National Science Foundation under Grants No. DMR-0554792 and No. DMR-1106230 as well as interim support from the Vice President for Research at the University of Virginia. P.P. and J.M.H. also acknowledge Professor Dr. Peter van Aken (MPI, Stuttgart) for inviting and allowing the author (P.P.) to use the SESAM.

*Formerly, Max Planck Institute for Metals Research, Heisenbergstrasse 3, 70569 Stuttgart, Germany.
†Corresponding author: jh9s@virginia.edu

[1] L. J. Sherry, R. Jin, C. A. Mirkin, G. C. Schatz, and R. P. Van Duyne, Nano Lett. **6**, 2060 (2006).
[2] J. Nelayah, M. Kociak, O. Stéphan, F. J. Garcia de Abajo, M. Tencé, L. Henrard, D. Taverna, I. Pastoriza-Santos, L. M. Liz-Marzan, and C. Colliex, Nat. Phys. **3**, 348 (2007).
[3] P. E. Batson, Solid State Commun. **34**, 477 (1980).
[4] M. Kociak, L. Henrard, O. Stéphan, K. Suenaga, and C. Colliex, Phys. Rev. B **61**, 13936 (2000).
[5] M. Moskovits, Science **332**, 676 (2011).
[6] A. Howie and R. H. Milne, Ultramicroscopy **18**, 427 (1985).
[7] Z. L. Wang, Micron **27**, 265 (1996).
[8] P. Moreau, N. Brun, C. A. Walsh, C. Colliex, and A. Howie, Phys. Rev. B **56**, 6774 (1997).
[9] M. Couillard, A. Yurtsever, and D. A. Muller, Phys. Rev. B **77**, 085318 (2008).
[10] E. W. D. Maclean, Ph.D. thesis, University of Glasgow, 2002.
[11] M. I. Stockman, Phys. Today **64**(2), 39 (2011).
[12] H. Reichert, M. Denk, J. Okasinski, V. Honkimäki, and H. Dosch, Phys. Rev. Lett. **98**, 116101 (2007).
[13] J. M. Howe, Philos. Mag. A **74**, 761 (1996).
[14] S. H. Oh, Y. Kauffmann, C. Scheu, W. D. Kaplan, and M. Rühle, Science **310**, 661 (2005).
[15] W. J. Huisman, J. F. Peters, M. J. Zwanenburg, S. A. de Vries, T. E. Derry, D. Abernathy, and J. F. van der Veen, Nature (London) **390**, 379 (1997).
[16] S. E. Donnelly, R. C. Birtcher, C. W. Allen, I. Morrison, K. Furuya, M. Song, K. Mitsuishi, and U. Dahmen, Science **296**, 507 (2002).
[17] S. K. Eswaramoorthy, J. M. Howe, and G. Muralidharan, Science **318**, 1437 (2007).
[18] K. Voitchovsky, J. J. Kuna, S. A. Contera, E. Tosatti, and F. Stellacci, Nat. Nanotechnol. **6**, 401 (2010).
[19] H. Reichert, O. Klein, H. Dosch, M. Denk, V. Honkimäki, T. Lippmann, and G. Reiter, Nature (London) **408**, 839 (2000).
[20] W. J. Huisman, Rev. Sci. Instrum. **68**, 4169 (1997).
[21] J. M. Howe and V. P. Oleshko, J. Electron Microsc. **53**, 339 (2004).
[22] J. J. Gilman, Philos. Mag. B **79**, 643 (1999).

[23]S. O. Kasap, *Principles of Electronic Materials and Devices* (McGraw-Hill, New York, 2006).
[24]I. B. Altfeder, J. A. Golovchenko, and V. Narayanamurti, Phys. Rev. Lett. **87**, 056801 (2001).
[25]S. G. Louie and M. L. Cohen, Phys. Rev. Lett. **35**, 866 (1975).
[26]G. D. Mahan and L. M. Woods, Phys. Rev. Lett. **80**, 4016 (1998).
[27]G. D. J. Smit, S. Rogge, and T. M. Klapwijk, Appl. Phys. Lett. **80**, 2568 (2002).
[28]R. Hillenbrand and F. Keilmann, Appl. Phys. Lett. **80**, 25 (2002).
[29]V. P. Oleshko and J. M. Howe, Ultramicroscopy **111**, 1599 (2011).
[30]R. F. Egerton, *Electron Energy-Loss Spectroscopy in the Electron Microscope* (Plenum, New York, 1996).
[31]B. Schaffer, W. Grogger, and G. Kothleitner, Ultramicroscopy **102**, 27 (2004).
[32]P. Palanisamy, Ph.D. thesis, University of Virginia, 2011.
[33]N. A. Belov, D. G. Eskin, and A. A. Aksenov, *Multicomponent Phase Diagrams: Applications for Commercial Aluminum Alloys* (Elsevier, Amsterdam, 2005).
[34]C. J. Powell, Phys. Rev. **175**, 972 (1968).
[35]P. Palanisamy and J. M. Howe, J. Appl. Phys. **110**, 024908 (2011).
[36]A. Howie and R. H. Milne, J. Microsc. **136**, 279 (1984).
[37]H. Raether, *Excitations of Plasmons and Interband Transitions by Electrons* (Springer-Verlag, Berlin, 1980).
[38]R. H. Ritchie, Phys. Rev. **106**, 874 (1957).
[39]D. A. Muller and J. Silcox, Ultramicroscopy **59**, 195 (1995).
[40]B. W. Reed and M. Sarikaya, Phys. Rev. B **64**, 195404 (2001).
[41]S. Lozano-Perez, J. Phys.: Conf. Ser. **126**, 012040 (2008).
[42]F. I. Allen, M. Watanabe, Z. Lee, N. P. Balsara, and A. M. Minor, Ultramicroscopy **111**, 239 (2011).
[43]G. Storaska, K. T. Moore, and J. M. Howe, Philos. Mag. **84**, 2619 (2004).
[44]A. R. Lupini and S. J. Pennycook, Ultramicroscopy **96**, 313 (2003).
[45]A. Berger, J. Mayer, and H. Kohl, Ultramicroscopy **55**, 101 (1994).
[46]C. T. Koch, W. Sigle, R. Höschen, M. Rühle, E. Essers, G. Benner, and M. Matijevic, Microsc., Microanal., Microstruct. **12**, 506 (2006).